Determining the physisorption energies of molecules on graphene nanostructures by measuring the stochastic emission-current fluctuation

Takahiro Matsumoto,[1,2,*] Yoichiro Neo,[2] Hidenori Mimura,[2] and Makoto Tomita[3]
[1]*Research and Development Center, Stanley Electric Corporation, 5-9-5 Tokodai, Tsukuba 300-2635, Japan*
[2]*Research Institute of Electronics, Shizuoka University, 3-5-1 Johoku, Hamamatsu 432-8011, Japan*
[3]*Department of Physics, Faculty of Science, Shizuoka University, 836 Ohya, Suruga 422-8529, Japan*
(Received 15 November 2007; published 25 March 2008)

A method of determining the physisorption energy of molecules on carbon nanostructures using field emission current fluctuation measurements is presented. A stochastic model, broken into birth and death processes, was applied to analyze the current fluctuation and determine the physisorption energy. This method yields a highly sensitive, precise determination of the physisorption energy of molecules, and we include the physisorption energies for various molecules on a graphene nanostructure.

DOI: 10.1103/PhysRevE.77.031611 PACS number(s): 68.37.Vj, 85.45.Db, 61.48.De, 02.50.−r

Zero-, one-, and two-dimensional carbon nanostructures have great potential in a broad range of applications ranging from molecular sensors [1–3] to field emission devices [4,5]. For example, understanding the adsorption and transport properties of molecules on or inside carbon nanostructures is of great importance for special items such as gas sensors [1–3] and nanovalves [6–8]. Numerous methods have been used to measure gas adsorption, including electric resistance (capacitance) [1,2,9,10] and thermal desorption [11,12]. However, these methods lack sensitivity and suffer from a slow response time.

The electronic properties of nanotubes are very sensitive to the adsorption of molecules [3,13–15]. This characteristic is clearly observed when measuring field emission-current fluctuations of carbon nanostructures, where the emission-current stability is easily lost under typical vacuum condition (10^{-8} Pa) with the introduction of trace amounts of gas (10^{-6} Pa). This phenomenon can be explained as the adsorption and desorption of molecules onto emission sites of carbon nanostructures with the molecules adsorbing onto the nanostructures affecting the electronic properties, such as charge transfer and tunneling probability [16,17].

In this paper, we report a method of determining the physisorption energy by measuring the field emission-current fluctuation. We present a model in which the field emission-current fluctuation originates from the adsorption and desorption of molecules onto a graphene nanoneedle, which is described using a stochastic birth and death model [18]. The emission-current fluctuation was analyzed as a function of cathode temperature using differential equations obtained from the model. Finally, we show how to determine the physisorption energy of various molecules on graphene surfaces accurately.

Graphene nanoneedles (GRANNs) were fabricated by hydrogen plasma etching a carbon rod. The 0.5-mm-diam rod was mechanically sharpened to a diameter of less than 10 μm at one end, and then the GRANNs were formed on the tip by hydrogen plasma etching. The hydrogen plasma etching was done using a radio frequency power of 800 W, a gas pressure of 10 Torr, a H_2 gas flow rate of 80 sccm, and a substrate temperature of 600 °C for about 30 min [19]. Before etching, the 0.5-mm-diam, mechanically sharpened, graphite rod had a smooth surface. After etching, the surface was covered with many nanoneedle structures with an aspect ratio on the order of 1000. A transmission electron microscopy (TEM) image of the spearhead region shows a single graphene nanoneedle structure (Fig. 1). The radius of curvature in the top region of the needle was less than 5 nm. This small radius and the high aspect ratio make it a suitable field electron emission source. Using high-resolution TEM, we observed a lattice fringe pattern from the bottom to the top of the needle. Based on the lattice fringe and diffraction patterns (*c* axis) shown in the inset of Fig. 1, the nanostructure consisted of a two-dimensional graphene sheet with an interplanar spacing of 0.36 nm. This value is larger than that of the hexagonal graphite structure (0.34 nm), indicating that the *c*-axis lattice is relaxed. Another diffraction pattern (*a* axis), orthogonal to the interplanar direction, was also observed. Based on the distance of the *a*-axis diffraction patterns, we determined that the atomic level of spacing was 0.21 nm. This value corresponds to the (010) plane spacing

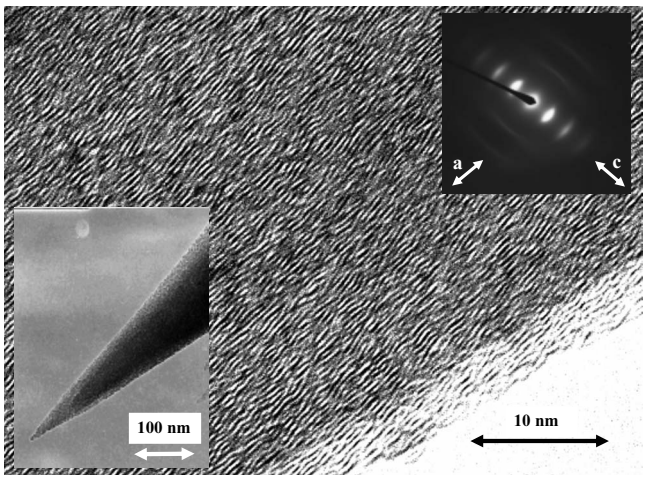

FIG. 1. TEM image (left inset), HRTEM image, and the selected area electron diffraction pattern (right inset) of a single graphene nanoneedle.

*Corresponding author; takahiro_matsumoto@stanley.co.jp

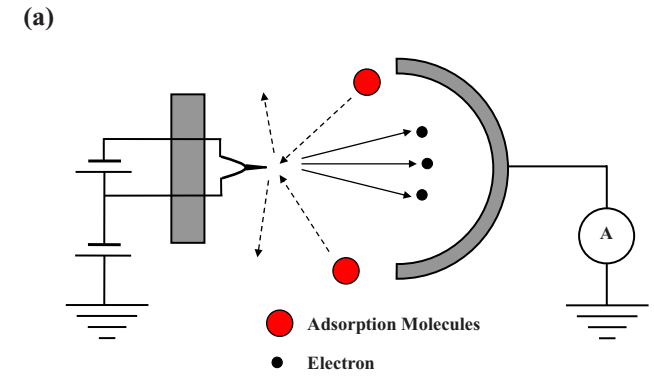

FIG. 2. (Color online) (a) Schematic diagram of the system used to measure fluctuation of the field emission current as a function of cathode temperature in the presence of various purified gases. (b) Physical desorption model in which fluctuation of the emission current originates from the adsorption and desorption of molecules onto the emission sites.

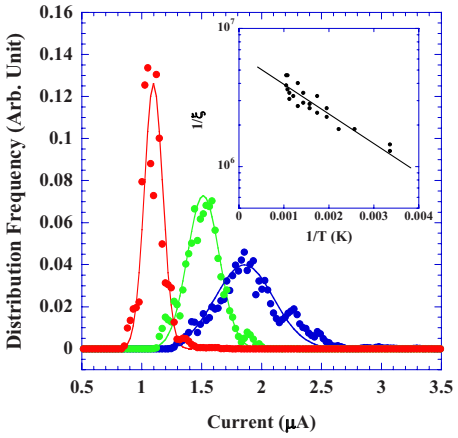

FIG. 3. (Color online) Histogram of the emission-current intensity at 300 K (rightmost, blue circles), 700 K (center, green circles), and 925 K (leftmost, red circles) in a H_2 atmosphere; the solid lines are the theoretically fitted curves. The inverse of the variance, $1/\xi$, for each temperature obtained by the theoretical fitting is shown as solid circles. The solid line is the fitted curve with a physical adsorption energy of 45 meV.

of the six-membered ring in the graphene sheet. The two-dimensional (2D) graphene sheet structure with the lattice fringes going from bottom to top is promising for electron field emission because of the exceptionally large carrier mobility (μ=15 000 $cm^2\ V^{-1}\ s^{-1}$) and the small electron mass (0.007 m_e, m_e being the free electron mass) [20–22].

The apparatus is shown schematically in Fig. 2(a). The field emission fluctuation current was measured as a function of cathode temperature in the presence of various purified gases, including H_2, CO, He, and Ar, at pressures of 10^{-4}–10^{-6} Pa over a temperature range of 300–1800 K. The system had a point-to-semisphere electrode geometry with the anode and field emitter separated by 10 cm. The fluctuation was measured with a picoammeter and recorded over 200 s with a 1 ms sampling period [23]. Ultrahigh purity (99.999%) gases were introduced through ultrahigh vacuum leak valves, and a high sensitivity quadrupole mass spectrometer monitored the gas pressure of the physisorbed species. The system was evacuated to a base pressure of 1×10^{-8} Pa before the measurements. The GRANN cathode was attached to a *W* filament using graphite dispersion to heat the cathode, and the temperature of the GRANN cathode was measured using a pyrothermometer or radiation thermometer. Electric potentials of 0 to −10 kV were applied between the cathode and anode to achieve field emission.

Figure 3 shows the fluctuating emission-current distribution measured in a 10^{-4} Pa H_2 atmosphere [24]. The probe current intensity distribution at 300 K shown in Fig. 3 (rightmost, blue circles) gives the current fluctuation deviation, $\Delta I/I_p$=0.31, where ΔI is the full width at half maximum (FWHM) of the fluctuation and I_p is the peak value of the current. Figure 3 shows the distributions of the fluctuating emission current at 700 K (center, green circles) and 925 K (leftmost, red circles). The deviation can be reduced by heating the cathode: $\Delta I/I_p$=0.21 at 700 K and $\Delta I/I_p$=0.16 at 925 K. This reduction in the deviation suggests that heating is an effective way to stabilize the field emission current. Along with the reduction of the deviation, the peak of the current distribution shifts to the lower current side with increasing cathode temperature. Both the reduction of the deviation and the lower peak shift of the current distribution can be interpreted qualitatively as the adsorption and desorption of atoms or ions on or off surface of the cathode [25,26].

Figure 2(b) illustrates the model in which the emission-current fluctuation originates from the adsorption and desorption of atoms and/or ions. The current fluctuation occurs due to the occupation of the emission sites by the adsorbed atoms. Here, we postulate that the magnitude of the current (I) is proportional to the number of occupied states (n); e.g., $I(n)=I_0+\eta n$, where I_0 is the emission current of an unoccupied state, and η is the magnitude of the current hop due to the adsorption of a single molecule, to explain both the reduction of the deviation and the lower peak shift of the current distribution. For this model, we define the transition probability of the number of adsorbed atoms from state E_i to state E_j as

$$P_{ij}(t) = P[X(s+t) = j | X(s) = i], \tag{1}$$

where $X(s)$ is a random variable at time s. We postulate that the system changes only through transitions from states to their nearest neighbors. If at time t, the system is in state E_i,

the probability that between t and $t+h$ the transition $E_i \rightarrow E_{i+1}$ occurs equals $\lambda_i h+o(h)$, and the probability of $E_i \rightarrow E_{i-1}$ equals $\mu_i h+o(h)$. The probability that during $(t,t+h)$ more than one change occurs is $o(h)$, where λ_i corresponds to the adsorption rate, μ_i corresponds to the desorption rate, $o(h)$ denotes a small quantity of the order of magnitude h, and h is the subinterval of time duration $h=1/N$ (N: total interval, and generally $h \rightarrow 0$). That is, the adsorption and desorption rates in state E_i can be written as:

$$P_{ii+1}(h) = \lambda_i h + o(h), \tag{2}$$

$$P_{ii-1}(h) = \mu_i h + o(h), \tag{3}$$

$$P_{ii}(h) = 1 - (\lambda_i + \mu_i)h + o(h), \tag{4}$$

$$P_{ik}(h) = o(h) \quad (|i-k| \geqslant 2), \tag{5}$$

$$P_{ij}(h) = \delta_{ij}. \tag{6}$$

We consider that the adsorption and desorption processes shown in Fig. 2(b) can be described quantitatively as time-homogeneous Markov processes satisfying the following Chapman-Kolmogorov equation [18]:

$$P_{ij}(t+h) = \sum_k P_{ik}(t)P_{kj}(h). \tag{7}$$

By taking $k=j-1$, j, $j+1$ for the summation in Eq. (7) and using Eqs. (1)–(6), we obtain the following differential equations:

$$\frac{dP_{ij}(t)}{dt} = \mu_{j+1}P_{ij+1}(t) + \lambda_{j-1}P_{ij-1}(t) - (\lambda_j + \mu_j)P_{ij}(t), \tag{8}$$

$$\frac{dP_{i0}(t)}{dt} = \mu_1 P_{i1}(t) - \lambda_0 P_{i0}(t). \tag{9}$$

To describe the adsorption and desorption processes shown in Fig. 2(b), we assume that the rate λ_j is proportional to the number of unoccupied emission sites, while the rate μ_j is proportional to the number of occupied sites. Defining N_0 as the total number of emission sites and j as the number of occupied sites, we set

$$\lambda_j = \alpha(N_0 - j), \tag{10}$$

$$\mu_j = \beta j, \tag{11}$$

where α and β are constants, such that α depends linearly on both the current density and the residual pressure and β depends on the temperature of the cathode. For example, $\beta \propto \exp[-E_{ad}/k_B T]$, where E_{ad} is the physical adsorption energy, T is the temperature, and k_B is the Boltzmann constant. Considering the stationary distribution for Eqs. (8)–(11), the limits $\lim P_{ij}(t)=p_j$, $t \rightarrow \infty$, exist and are independent of the initial conditions [27]. Therefore, Eqs. (8)–(11) can be combined to express the stationary distribution p_n as the following Poisson distribution:

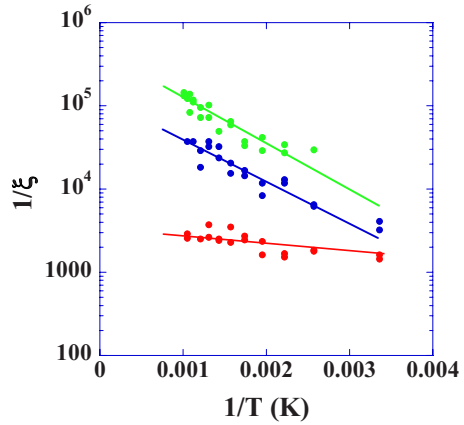

FIG. 4. (Color online) Inverse of the variance, $1/\xi$, for CO molecules (top, green circles), Ar molecules (center, blue circles), and He molecules (bottom, red circles) as a function of GRANN cathode temperature. The solid lines are the fitted curves with physical adsorption energies of 110 meV for CO molecules, 100 meV for Ar, and 15 meV for He.

$$p_n = \frac{\xi^n}{n!}\exp(-\xi), \tag{12}$$

where $\xi=N_0\alpha/(\alpha+\beta)$ and we assume the desorption ratio, β, is much larger than the adsorption ratio, α.

The solid lines in Fig. 3 are the theoretically fitted curves given by Eq. (12), where the best fits were obtained using the fitted values, $\xi=2.76\times10^{-7}$ for 920 K (leftmost, red line), $\xi=3.45\times10^{-7}$ for 700 K (center, green line), and $\xi=7.72\times10^{-7}$ for 300 K (rightmost, blue line). By fitting the histogram of the current fluctuation at various cathode temperatures with Eq. (12), and then plotting these theoretically determined values logarithmically $[\ln(1/\xi)]$ as a function of the inverse of the temperature, $1/T$, we can determine the physical adsorption energy, E_{ad}, from the slope, as shown in the inset of Fig. 3. The solid line shown in the inset of Fig. 3 is the theoretical line computed with a physisorption energy of $E_{ad}=45$ meV. The adsorption energies of H_2 molecules on graphitelike surfaces show a wide range of binding energies from 20 to 80 meV [28,29] because the adsorption energy of molecules on the carbon nanostructures varies as the size (e.g., the tube diameter), coordinate sites, and the surface structure of the carbon nanomaterials change. We cannot distinguish the adsorption sites of the H_2 molecules onto the emission sites of the carbon nanostructures; however, the physisorption energy of $E_{ad}=45$ meV is similar to the energy onto a graphite surface [30], leading to our conclusion that the electron emission occurs not from the edge of the nanoneedle, but from the basal plane where the crystal structure is similar to the graphite surface.

The error obtained by this method is within ± 5 meV, which allows the determination of the physisorption energy of various molecules to a high degree of accuracy. Figure 4 shows the values of $1/\xi$ obtained by measuring the emission-current fluctuations as a function of various temperatures for CO (top, green circles), Ar (center, blue circles), and He molecules (bottom, red circles). The slope of the solid line

shows the theoretically determined physical adsorption energies, E_{ad}: 110 meV for CO molecules, 100 meV for Ar, and 15 meV for He. These graphene nanoneedle physisorption energies are similar to the physisorption energies for the graphite surface [30]. We cannot rule out the possibility that the current fluctuation occurs due to variations in the adsorbate coverage on step edges and defects, where the enhancement of physisorption energy occurs [31,32]. However, polar adsorbates such as CO molecules on the graphite nanostructure showed similar adsorption energy to those on the graphite basal surface, and we did not observe enhancement of the binding energy due to a dipole interaction between polar molecules and step edges or defects. Therefore, we consider that the electron emission occurs not from the edge of the nanoneedle, but from the basal plane of the graphene sheet.

In conclusion, we have presented a stochastic model with birth and death processes to describe the emission-current fluctuation originating from the adsorption and desorption of molecules onto the emission sites, and have determined the physisorption energies of various molecules on a graphene sheet nanostructure. The region of the emission sites (i.e., the localized region of the electron wave function) affected by this molecule physisorption is still an open question.

[1] E. S. Snow and F. K. Perkins, Nano Lett. **5**, 2414 (2005).

[2] E. S. Snow, F. K. Perkins, E. J. Houser, S. C. Badescu, and T. L. Reinecke, Science **307**, 1942 (2005).

[3] J. Kong, N. Franklin, C. Zhou, M. G. Chapline, S. Peng, K. Cho, and H. Dai, Science **287**, 622 (2000).

[4] T. Matsumoto and H. Mimura, Appl. Phys. Lett. **82**, 1637 (2003).

[5] T. Matsumoto and H. Mimura, Appl. Phys. Lett. **84**, 1804 (2004).

[6] Y. Maniwa, K. Matsuda, H. Kyakuno, S. Ogasawara, T. Hibi, H. Kadowaki, S. Suzuki, Y. Achiba, and H. Kataura, Nat. Mater. **6**, 135 (2007).

[7] J. K. Holt, H. G. Park, Y. Wang, M. Stadermann, A. B. Artyukhin, C. P. Grigoropoulos, A. Noy, and O. Bakajin, Science **312**, 1034 (2006).

[8] G. Hummer, J. C. Rasaiah, and J. P. Noworyta, Nature (London) **414**, 188 (2001).

[9] J. A. Robinson, E. S. Snow, S. C. Badescu, T. L. Reinecke, and K. Perkins, Nano Lett. **6**, 1741 (2006).

[10] L. Valentini, F. Mercuri, I. Armentano, C. Cantalini, S. Picozzi, L. Lozzi, S. Santucci, A. Sgamellotti, and J. M. Kenny, Chem. Phys. Lett. **387**, 356 (2004).

[11] A. C. Dillon, K. M. Jones, T. A. Bekkedahl, C. H. Klang, D. S. Bethune, and M. J. Heben, Nature (London) **386**, 377 (1997).

[12] N. Chakrapani, Y. M. Zhang, S. J. Nasyak, J. A. Moore, D. L. Carroll, Y. Y. Choi, and P. M. Ajayan, J. Phys. Chem. B **107**, 9308 (2003).

[13] J. Zhao, A. Buldum, J. Han, and J. P. Lu, Nanotechnology **13**, 195 (2002).

[14] M. Grujicic, G. Cao, and R. Sigh, Appl. Surf. Sci. **211**, 166 (2003).

[15] J. Andzelm, N. Govind, and A. Maiti, Chem. Phys. Lett. **421**, 58 (2006).

[16] W. P. Dyke and W. W. Dolan, Adv. Electron. Electron Phys. **8**, 89 (1956).

[17] J. W. Gadzuk and E. W. Plummer, Rev. Mod. Phys. **45**, 487 (1973).

[18] W. Feller, *An Introduction to Probability Theory and its Application*, 3rd. ed. (John Wiley & Sons, New York, 1957), Vol. 1, p. 444.

[19] T. Matsumoto and H. Mimura, J. Vac. Sci. Technol. B **23**, 831 (2005).

[20] K. S. Novoselov, A. K. Geim, S. V. Morozov, D. Jiang, M. I. Katsnelson, I. V. Grigorieva, S. V. Dubonos, and A. A. Firsov, Nature (London) **438**, 197 (2005).

[21] Y. Zhang, Y. W. Tan, H. L. Stormer, and P. Kim, Nature (London) **438**, 201 (2005).

[22] A. K. Geim and K. S. Novoselov, Nat. Mater. **6**, 183 (2007).

[23] The sampling period was determined so as not to measure more than one change during this time interval.

[24] We used the current step η of the histogram as 25 nA, which was decided by $\eta=[I(N_0)-I_0]/N_0$, where both the maximum and minimum emission currents $I(N_0)=3.5\ \mu$A and $I_0=0.5\ \mu$A were determined by the field emission-current measurements, and the number of emission sites N_0 was decided as $N_0=100$ by our field emission microscope measurements.

[25] S. Yamamoto, S. Hosoki, S. Fukuhara, and M. Futamoto, Surf. Sci. **86**, 734 (1979).

[26] S. Hosoki, S. Yamamoto, M. Futamoto, and S. Fukuhara, Surf. Sci. **86**, 723 (1979).

[27] In this model, the emission current distribution depends on both the initial current setting and the gas pressure. Therefore, both states E_i and E_j are considered. However, the adsorption energy derived by this model does not depend on the initial conditions. Therefore, it is much simpler to consider a single state E_j at time t as $P_j(t,t'+dt')=(1-\mu_j dt'-\lambda_j dt')P_j(t,t')+\mu_{j+1}P_{j+1}(t,t')+\lambda_{j-1}P_{j-1}(t,t')$.

[28] N. Jacobson, B. Tegner, E. Schroeder, P. Hyldgaard, and B. I. Lundqvist, Comput. Mater. Sci. **24**, 273 (2002).

[29] F. Tran, J. Weber, T. Wesolowski, F. Cheikh, Y. Ellinger, and F. Pauzat, J. Phys. Chem. B **106**, 8689 (2002).

[30] G. Vidali, G. Ihm, H. Kim, and M. W. Cole, Surf. Sci. Rep. **12**, 133 (1991).

[31] H. Ulbricht, G. Moss, and T. Hertel, Phys. Rev. B **66**, 075404 (2002).

[32] H. Ulbricht, R. Zacharia, N. Cindir, and T. Hertel, Carbon **44**, 2931 (2006).